Inter-decadal variation of the Tropical Atlantic – Korea (TA-K) teleconnection pattern during boreal summer season

Yoo-Geun Ham[1], YeonJi Hwang[1], Young-Kwon Lim[2], and Minho Kwon[3]

[1]Faculty of Earth Systems and Environmental Sciences, Chonnam National University, Gwangju, South Korea
[2]Goddard Earth Sciences Technology and Research/I. M. Systems Group, Global Modeling and Assimilation Office, NASA
[3]Ocean Circulation and Climate Research Center, Korea Institute of Ocean Science and Technology, Ansan, Korea

November 2017

Climate Dynamics (1st Revision)

*Corresponding author: Yoo-Geun Ham, Faculty of Earth Systems and Environmental Sciences, Chonnam National University, 77 Yongbong-ro, Buk-gu, Gwangju 500-757, Republic of Korea (ygham@jnu.ac.kr)

Abstract

The inter-decadal variation of the positive relationship between the tropical Atlantic sea surface temperature (SST) and Korean precipitation during boreal summer season during 1900–2010 is examined. The 15-yr moving correlation between the Tropical Atlantic SST (TAtlSST) index (SST anomalies from 30° S to 30° N and 60° W to 20° E) and Korean precipitation (precipitation anomalies from 35–40° N and 120–130° E) during June-July-August (JJA) exhibits strong inter-decadal variation, which becomes positive at the 95% confidence level after the 1980s. Intensification of the linkage between the TAtlSST index and Korean precipitation after the 1980s is attributed to global warming via the increased background SST. The increase in the background SST over the Atlantic provides background conditions that enhance anomalous convective activity by anomalous Atlantic SST warming. Therefore, the overall atmospheric responses associated with the tropical Atlantic SST warming could intensify.

The correlation between the TAtlSST index and Korean precipitation also exhibits strong inter-decadal variation within 1980–2010, which is over 0.8 during early 2000s, while it is relative low (i.e., around 0.6) during the early 1980s. The enhanced co-variability between the tropical and the mid-latitude Atlantic SST during the early 2000s induces a TAtlSST-related Rossby wave source over the mid-latitude Atlantic, which excites stationary waves propagated from the Atlantic to the Korean peninsula across northern Europe and northeast Asia. This Rossby-wave train induces a cyclonic flow over the northern edge of the Korea, which intensifies southwesterly and results in precipitation over Korea. This observed decadal difference is well simulated by the stationary wave model experiments with a prescribed TAtlSST-related Rossby wave source over the mid-latitude Atlantic.

1. Introduction

The major rainy season during boreal summer in Korea, which has two rainfall-peaks (between late June and late July, and between mid-August and early September), is called *Changma* (Wang et al., 2007; Ho and Kang, 1988; Lim et al., 2002; Seo et al., 2011; Lee et al., 2017). As an important component of the East Asia summer monsoon (EASM) system, the climatological evolution of Changma is closely linked to the summer monsoon rainfall band across east Asia, which leads major rainfall in China (i.e., Mei-yu) and Japan (i.e., Baiu). However, the variability of Changma is known to be rather different from Mei-yu or Baiu due to its more complex mechanisms (Seo et al., 2011; Jeong et al., 2017).

While inter-annual variation of rainfall anomalies during boreal summer in China or Japan is known to be determined by the large-scale sea surface temperature (SST) over the tropical Pacific (e.g., the El Niño Southern Oscillation: ENSO; Huang and Wu, 1989; Wu et al., 2010), it is not clear whether the Pacific SST can lead to variation in summer rainfall in Korea (Chen and Zhou, 2014; He and Zhou, 2014). For example, Yun et al. (2014) used empirical orthogonal function (EOF) analysis to show that the first EOF of the summer-averaged convection anomalies over Asia is controlled by the tropical Pacific SST, and that the first EOF exhibits a contrast pattern in the convection activity between China and Japan, while the convection anomalies over Korea are relatively weaker. In addition, Son et al. (2014, 2015) found that a significant statistical relationship between Korean precipitation and the ENSO is shown during the September and boreal-winter development of El Nino, while the summer Korean precipitation is weakly correlated to the ENSO.

The role of the Indian Ocean on the summer monsoon over East Asia is known to some extent. Basin-wide Indian Ocean warming is reported to affect the inter-annual variability of the

rainfall over the western north Pacific and Japan through the Pacific-Japan (PJ) pattern (Kosaka and Nakamura, 2006; Kosaka et al., 2013). This is further supported by the Atmospheric Global Climate Model (AGCM) experiments (Annamalai et al., 2005; Yang et al., 2007). However, the relationship between the PJ pattern and Korean precipitation is known to be marginal (Kosaka et al., 2013). The intensity of Changma is controlled by the intensity of the Indian summer monsoon (ISM) by energy variation of the circumglobal teleconnection (CGT) pattern (Ding et al., 2011; Wang et al., 2012; Lee and Ha, 2015).

While the dynamic role of the Pacific or Indian Ocean on the summer precipitation variability over Korea has been actively investigated for the past several decades, studies on the role of the Atlantic Ocean only started in recent years. Recently, Ham et al. (2017) found a strong relationship between Korean precipitation and the tropical Atlantic SST during boreal summer. They showed that the relationship is quite robust from early to late summer. They argued that the positive Atlantic SST anomaly could induce a reduction in the convective anomalies over the western Pacific by modulating the Walker Circulation. This excites the low-level anti-cyclonic flow over the western north Pacific (i.e., Western-North Pacific Subtropical High, WNPSH). This leads the southerly to advect wet air to Korea, which enhances precipitation. This atmospheric bridge is quite different from the atmospheric bridge from the north Atlantic to Eurasia, which involves the Rossby wave train from the north Atlantic to Eurasia (Wu et al., 2010, 2011; Lim, 2015; Ye et al., 2015).

This relationship between the tropical Atlantic SST and Korean summer precipitation varies strongly on a decadal time scale. In Lee et al. (2017), it is pointed out that the 15 yr moving correlation between the tropical Atlantic SST and Korean summer precipitation was negative during the early 1900s, but showed a sudden change to exhibit a significant positive relationship

after the 1980s (see their Fig. 9, and also Fig. 1a in this paper). Specifically, the correlation is > 0.8 for around the 2000s, which denotes that more than 60% of the total Korean-precipitation variability might be explained by the TAtlSST variability during boreal summer. However, the dynamic mechanism of this strong inter-decadal variation of the Tropical Atlantic-Korea (TA-K) teleconnection pattern has never before been examined.

Therefore, this study investigates the decadal modulation of the tropical Atlantic-Korea teleconnection pattern using reanalysis data. In section 2, observational data and the model used in this study are summarized. Section 3 provides the mechanism of the decadal-variation of the Tropical Atlantic-Korea (TA-K) teleconnection pattern. A summary and discussion are provided in Section 4.

2. Data and Models

a. Observational data

In this study, we used two datasets for precipitation. For land precipitation, the data used for the Korean Peninsula precipitation index (Figure 1) during 1901–2011 was from the Climate Research Unit (CRU, Harris et al., 2013). The Global Precipitation Climatology Project (GPCP, Adler et al., 2003) precipitation data during 1979–2008 was used for linear regression analysis. The observed sea surface temperature (SST) data during 1901–2011 was from the NOAA Extended Reconstructed Sea Surface Temperatures version 3 (ERSST V3b, Smith et al., 2008). The 500 hPa vertical pressure velocity data, 850 hPa zonal and meridional wind data during 1948–2010, and 500 hPa geopotential height data during 1979–2008 were from the National Center for Environmental Prediction/National Center for Atmospheric Research (NCEP/NCAR)

120 reanalysis version 1 (NCEP1, Kalnay et al., 1996). All data were linearly de-trended before
121 analysis.
122
123 *b. The Stationary Wave Model (SWM)*
124 We use the SWM to investigate large-scale atmospheric response to the Rossby wave
125 sources found in the North Atlantic. This SWM is the dry dynamical core of a fully nonlinear
126 time-dependent baroclinic model (Ting and Yu, 1998; Schubert et al., 2011). It has three-
127 dimensional (3-D) primitive equations in σ coordinates with 14 unevenly spaced vertical levels.
128 Horizontally, the model has rhomboidal wavenumber-30 truncation. A rigid-lid boundary
129 condition is applied at the top and at the surface of the model atmosphere. For damping,
130 Rayleigh friction and Newtonian cooling are applied in the vorticity, divergence, and temperature
131 equations to ensure meaningful solutions (Ting and Yu, 1998; Lim, 2015).
132 Vorticity induced by divergent (irrotational) flow forces the model to generate a large-scale
133 rotational component of the atmospheric circulation in the form of Rossby wave propagation. In
134 our study, we estimated the regressed Rossby wave source in the TAtlSST index using
135 NCEP/NCAR re-analysis data. The SWM is forced by this Rossby wave source. The vertical
136 profile of the Rossby wave source has a maximum in the upper-troposphere (Liu et al., 1998).
137 The background basic state for the model is given by three dimensions globally from surface to
138 tropopause. With these configurations, the model generates large-scale wave trains across
139 Eurasia in response to the Rossby wave source in the North Atlantic (e.g., Fig. 8). For further
140 details of the model, see Ting and Yu (1998).
141
142 **3. Mechanism of the inter-decal variation of the Tropical Atlantic-Korea (TA-K)**

teleconnection pattern

Figure 1a shows the 15-yr moving correlation between the precipitation anomaly over the Korean peninsula from 35–40° N and 120–130° E, and the Tropical Atlantic SST (TAtlSST) index, defined as an area-averaged sea surface temperature (SST) from 30° S to 30° N and 60° W to 20° E, during Korean summer (June-July-August: JJA). During the first half of the 20th century, the correlation between Korean precipitation and the TAtlSST index varies from −0.5 to zero at the 95% confidence level. For example, the correlation for 1910–1920 is negative, while the correlation for 1920–1950 is nearly zero. The correlation during the 1960s is positive, but becomes nearly zero for 1970–1980. However, after the mid-1980s, the correlation changed abruptly to a significantly positive value at > 95% confidence. This indicates that the positive relationship between the tropical Atlantic SST and Korean precipitation during boreal summer became significant after the 1980s. To demonstrate clearly the decadal variation of the relationship between the TAtlSST and Korean precipitation, in Figure 1b (and with black dots in Fig. 1c) the scatter plot shows Korean precipitation and the TAtlSST index for 1948–1978 and 1979–2010, respectively. During 1948–1978, the correlation between the TAtlSST index and the Korean precipitation is only −0.19, while that during 1979–2010 is 0.58 with > 95% confidence. Hereafter, the periods 1948–1978 and 1979–2010 are denoted P1 and P2.

It is also interesting that the maximum 15-yr moving correlation is slightly > 0.8 around 2000 (red dots in Fig. 1a). This means that about 65% of the total variability in precipitation over Korea during boreal summer occurs during this period. The red and blue dots in Fig. 1c show that the correlation between the TAtlSST index and Korean precipitation during 1994–2008 is > 0.8, while that during 1979–1993 is 0.63. This means that the relationship between the tropical Atlantic and Korean precipitation also varies after 1980s even though it continuously exhibits

significantly positive values. To assess the details of mechanisms of the decadal variation of the Tropical Atlantic-Korea (TA-K) teleconnection pattern after 1980s, the period 1979–1993 is denoted P3, while 1994–2008 is denoted P4.

a. Decadal difference between P1 and P2

To demonstrate the systematic difference associated with the TAtlSST index between P1 and P2, Figure 2 shows the regression of the SST, vertical pressure velocity at 500 hPa, wind-vector and stream function at 850 hPa during 1948–1978 (P1) and 1979–2010 (P2). During P1, the regressed SST anomalies show a positive signal with anomalous upward motion over the equatorial Atlantic (Fig. 2a, 2b). The anomalous upward motion is closely linked to the release of latent heat by the condensation of water vapor, which heats the atmospheric and induces Gill-type atmospheric circulation anomalies (Gill, 1980). As a result, low-level cyclonic circulations are induced north and south (a pair) of the equatorial Atlantic. The weaker cyclonic circulation over the region south of the equatorial Atlantic is probably associated with the location of the anomalous convection, which is north of the equator with the northward shift of the Atlantic Intertropical Convergence Zone (ITCZ) during boreal summer.

Ham et al. (2017) showed that the SST warming over the tropical Atlantic triggers the low-level easterly wind anomaly over the maritime continent by modulating the zonal Walker circulation. This leads the low-level divergence over the western Pacific to decrease the precipitation anomalies. The negative atmospheric heating anomaly excites a low-level anti-cyclonic circulation over the sub-tropical western Pacific. This is consistent with many previous studies indicating that the tropical Atlantic SST can lead the equatorial easterly over the western Pacific (Ding et al., 2010; Rong et al., 2010; Ham et al., 2013a,b). Consistent with previous

189 studies, an anti-cyclonic circulation is shown over the western-north Pacific (Figure 2c).

190 During P2, the positive SST anomalies over the Atlantic extend farther to the north
191 compared to those during P1. For example, the positive SST anomalies during P1 are nearly zero
192 north of 15° N, while the positive SST anomalies related to the TAtlSST index during P2 extend
193 to 30° N (Fig. 2d). In addition, the positive SST anomalies are clear over the mid-latitude and
194 north Atlantic, with weak negative SST anomalies over the mid-latitude western Atlantic.
195 Consistent with the positive SST anomalies over the tropical Atlantic, local anomalous upward
196 motion is shown clearly during P2 (Fig. 2e). The dramatic differences from P1 during P2 are the
197 responses of the atmospheric circulation over the Pacific. During P2, the low-level anti-cyclonic
198 flow associated with the TAtlSST index is well-induced over the western Pacific (Fig. 2f). The
199 low-level anti-cyclonic circulation leads the southerly over the Korean peninsula; then, induces
200 the anomalous upward motion that is the signal of increased precipitation.

201 The enhancement of the anti-cyclonic flow over the western Pacific associated with the
202 tropical Atlantic SST during P2 is consistent with previous studies (Rodionov, 2004; Hong et al.,
203 2014). Hong et al. (2014) revealed that the tropical Atlantic SST contributes significantly to the
204 intensified variability of the western-north Pacific subtropical high (WNPSH) after the early
205 1980s. Hong et al. (2014) also argued that the weakened positive relationship between the ENSO
206 and the SST over the tropical Atlantic is responsible for the intensified role of tropical Atlantic
207 SST on the WNPSH after the early 1980s. That is, when there is strong coupling between El
208 Nino and the tropical Atlantic SST, the low-level anti-cyclonic flow over the subtropical western
209 Pacific (induced by the tropical Atlantic SST) is cancelled by the cyclonic flow due to the El
210 Nino signal over the equatorial eastern Pacific.

211 In addition, they suspected that the difference in changes of mean state between P1 and P2

might contribute to enhancing WNPSH with tropical Atlantic SST warming; however, they left the resolution of this issue for future work. To examine this point in more detail, Figure 3 shows the background state difference of the SST and vertical pressure velocity at 500 hPa between P2 and P1. Due to the global warming in recent decades, the overall background SST in P2 was systematically higher than that in P1. In particular, the increase in the SST over the Atlantic, Indian Ocean, and equatorial and subtropical western Pacific during P2 was more robust than in other regions. This implies that the increase in the background SST associated with global warming might be related to the enhanced TA-K teleconnection observed in recent decades. With the aid of the increased SST during P2, the background upward motion was enhanced over the equatorial Atlantic and western Pacific. On the other hand, the background upward motion over the central Africa and the equatorial central Pacific, where the increase of the background SST is relatively weak, was systematically weakened.

To compare the background state difference related to the enhancement of the TA-K teleconnection and global warming in more detail, Figure 4a and b show the linear trend of the background SST and the vertical pressure velocity from 1948 to 2010. As shown in Fig. 3, the linear trend of increase in the background SST over the Atlantic, Indian Ocean, and western Pacific is clear. In addition, the positive SST trend over the eastern Pacific, and the negative SST trend over the north Pacific are also shown. The linear trend of the vertical pressure velocity exhibits enhanced upward motion over the regions with greater positive trends in SST. For example, the negative vertical pressure velocity trend (i.e., enhanced upward motion) is robust over the Indian Ocean, western Pacific, and the Atlantic; while the positive vertical pressure velocity trend is shown over the equatorial central Pacific, where the linear SST trend is relatively weak.

Figure 4c and d show the regressed 15 yr moving background SST and the vertical pressure velocity at 500 hPa over the 15 yr moving correlation between the TAtlSST index and Korean precipitation. Therefore, the spatial distribution of the regression is understood to denote the background state difference to amplify the correlation between the TAtlSST index and Korean precipitation. Note that the regression was performed for the period 1948–2010 due to data limitation. Also, the student t-test for the regression line is performed for Fig. 4c, and 4d, and the area over 95% confidence level are only shaded. The positive signal in the background SST over the Atlantic, Indian Ocean, and eastern Pacific is shown clearly, implying that increase in the background SST over those regions can enhance the relationship between the tropical Atlantic SST and Korean precipitation. In addition, the enhanced upward motion over the tropical Atlantic, and Indian Ocean/maritime continent, and the weakened upward motion over the equatorial central Pacific, is associated with enhanced TA-K teleconnection. Those general features are quite similar to the spatial distribution of the linear trend. For example, the pattern correlation between the spatial distribution of the linear trend and that related to the enhanced TA-K teleconnection over the tropics (from 30° S to 30° N, and 0–360° E) is significant at > 99% confidence (i.e., 0.64 and 0.80 for the SST and the vertical pressure velocity, respectively). This implies that global warming possibly plays an important role in enhancing the linkage between the tropical Atlantic and the climate variability over the Korean peninsula.

Given this, how can the change in background state due to global warming amplify the atmospheric signals related to the tropical Atlantic SST? The impact of the background state on the atmospheric variability over the tropics has been investigated in previous studies (Choi et al., 2011; Chung and Li, 2013; Ham et al., 2013; Ham and Kug, 2012, 2015, 2016). Ham and Kug (2015) showed that simulation of the ENSO-related precipitation among climate models is linked

closely to that in the tropical mean state. They argue that the warmer background SST over the equatorial central-eastern Pacific enhances local anomalous convective activity during the El Nino, implying a positive relationship between wetness in the background state and El Nino-related precipitation anomalies. Consistent with the previous view, Choi et al. (2011) showed that the decades with warmer background SST over the tropical western Pacific helped to induce stronger local precipitation response to the SST anomaly; and therefore, led to much more frequent central Pacific-type El Ninos. This implies that the warmer background state over the tropical Atlantic can enhance anomalous convective activities and the resultant teleconnections induced by the tropical Atlantic SST anomaly.

To examine whether the background SST can influence the upward motion response to the SST anomaly, Fig. 5a shows a scatter diagram of the 15-yr moving SST and the anomalous vertical pressure velocity regressed onto the SST anomaly over the tropical Atlantic. Note that the regressed vertical pressure velocity anomaly indicates how strongly the atmospheric upward motion is induced due to the given SST forcing (Choi et al., 2011; Ham and Kug, 2015). It is clearly shown that the warmer background SST over the tropical Atlantic can lead stronger anomalous upward motion (i.e., negative vertical pressure velocity) forced by unit SST anomaly. With aids of higher background SST during P2, the overall atmospheric response to the TAtlSST is systematically stronger than that during P1, confirming that the warmer background SST during P2 provides a background state favorable to induction of a stronger local convection response to the tropical Atlantic SST anomaly.

In addition to the background SST over the tropical Atlantic, it was found that the warmer background SST over the warm pool region plays some role in amplifying the TA-K teleconnection. Hong et al. (2013) clearly showed through idealized AGCM experiments that the

atmospheric response over the tropical Pacific to the tropical Atlantic SST anomaly is strongly dependent on the location of the climatological warm pool. According to their experiments, the positive precipitation response to the tropical Atlantic SST anomaly is robust where the idealized warm pool is located. They argued that the climatological low-level convergence resulting from the warm pool over the western Pacific could lead strong low-level convergence feedback; therefore, the anomalous precipitation response could easily be amplified over the warm-pool region (Wang, 2000). This indicates that the warmer climatology over the warm pool could also amplify the Atlantic-induced teleconnection pattern over the Pacific.

To confirm this point, Figure 5b shows the scatter diagram between the 15 yr moving background SST over the warm pool region (from 5° S to 10° N and 100–140° E) and the anomalous zonal wind at 850 hPa over the western Pacific (from 5° S to 10° N and 130–160° E) regressed onto the TAtlSST index. To some extent, that notion that the TAtlSST-related easterly over the western Pacific tends to be enhanced during decades with warmer background state over the warm-pool region is supported. The stronger easterly over the western Pacific is linked to the anti-cyclonic flow over the subtropical western Pacific. This leads the southerly to increase the precipitation over the Korean peninsula.

As a short summary, the background SST increase due to global warming can enhance the TA-K teleconnection pattern by amplifying 1) the anomalous TAtlSST-related convective activity over the tropical Atlantic, and 2) the TAtlSST-related wind response over the equatorial western Pacific. The first feature is related to the increased background SST over the tropical Atlantic, and the second feature is related to the increased SST over the warm-pool region.

b. Decadal difference between P3 and P4

Figure 6 shows the regressed JJA SST, precipitation, and 850 hPa wind-vector anomalies onto the TAtlSST index during 1979–1993 (P3) and 1994–2008 (P4). The general SST warming over the tropical Atlantic from 30° S to 30° N is clearly shown in both periods. The SST warming over the equatorial eastern Atlantic from 5° S to 5° N was slightly stronger during P3. On the other hand, the SST warming over the western Atlantic between 10–30° N was stronger during P4, which lead stronger positive precipitation anomalies over the equatorial Atlantic. The stronger TAtlSST-related precipitation anomalies over the equatorial Atlantic can lead to the enhanced atmospheric responses over the western Pacific as discussed in a previous sub-section. That is, the easterly anomalies over the equatorial western Pacific, along with the southerly along the east coast of the China, are systematically stronger during P4. This could contribute to a stronger positive precipitation anomaly over Korea during P4.

In addition, the tripolar SST pattern over the Atlantic (related to warming over the tropical, north, and mid-latitude eastern Atlantic) and weak negative SST anomaly over the mid-latitude western Atlantic are clear in both periods, implying strong co-variability between the tropical and mid-latitude Atlantic SST (Lau and Nath, 2001; Czaja and Marshall, 2001; Czaja and Frankignoul, 2002; Huang and Shukla, 2005; Li et al., 2007). The TAtlSST-related SST warming over the mid-latitude eastern Atlantic was enhanced during P4 more than during P3, indicating that the co-variability between the tropical and the mid-latitude Atlantic became stronger during P4. The SST warming during P4 reached > 2 °C in the mid-latitude eastern Atlantic, while it was between 1 and 2 °C during P3. As a result, the enhanced SST warming over the mid-latitude Atlantic during P4 increased the local precipitation anomalies. That is, the precipitation anomalies regressed onto the TAtlSST index appeared negative over the mid-latitude Atlantic from 30–40° N during P3 (red box in Fig. 6b), while the positive precipitation anomalies became

more apparent during P4 (red box in Fig. 6d).

Those differences in the TAtlSST-related precipitation anomalies over the mid-latitude Atlantic could modify the teleconnection originating from the high-latitude wave source over the Atlantic. To examine the high-latitude teleconnection related to the TAtlSST index during P3 and P4, the geopotential height and the wave activity flux at 500 hPa related to the TAtlSST index was calculated for P3 and P4 (Fig. 7). The wave activity flux was calculated as follows (Takaya and Nakamura, 2001; Kosaka and Nakamura, 2006).

$$\mathrm{W} = \frac{p\cos\phi}{2|U|}\begin{pmatrix} \frac{U}{a^2\cos^2\phi}\left[\left(\frac{\partial\psi'}{\partial\lambda}\right)^2 - \psi'\frac{\partial^2\psi'}{\partial\lambda^2}\right] + \frac{V}{a^2\cos\phi}\left[\frac{\partial\psi'}{\partial\lambda}\frac{\partial\psi'}{\partial\phi} - \psi'\frac{\partial^2\psi'}{\partial\lambda\partial\phi}\right] \\ \frac{U}{a^2\cos^2\phi}\left[\frac{\partial\psi'}{\partial\lambda}\frac{\partial\psi'}{\partial\phi} - \psi'\frac{\partial^2\psi'}{\partial\lambda\partial\phi}\right] + \frac{V}{a^2}\left[\left(\frac{\partial\psi'}{\partial\phi}\right)^2 - \psi'\frac{\partial^2\psi'}{\partial\phi^2}\right] \\ \frac{f_0^2}{N^2}\left\{\frac{U}{a\cos\phi}\left[\frac{\partial\psi'}{\partial\lambda}\frac{\partial\psi'}{\partial z} - \psi'\frac{\partial^2\psi'}{\partial\lambda\partial z}\right] + \frac{V}{a}\left[\frac{\partial\psi'}{\partial\phi}\frac{\partial\psi'}{\partial z} - \psi'\frac{\partial^2\psi'}{\partial\phi\partial z}\right]\right\} \end{pmatrix} + C_U M \quad (1)$$

, where U, V denote the 15-yr averaged zonal, meridional wind, respectively. And, ψ', a, λ, ϕ, z denote the streamfunction regressed onto TAtlSST index, a radius of the earth, longitude, latitude, and vertical direction, respectively. The zonal, and the meridional components of the wave activity flux denote the zonal, and the merdional advection of the wave-activity (angular) pseudomomentum (Takaya and Nakamura, 2001).

During P3, the negative geopotential height anomaly over Europe and eastern Russia and the positive geopotential height anomaly over western Russia, were clear. The geopotential height anomalies over Korea exhibited slightly positive values. The wave activity flux indicates that geopotential height anomalies over Europe and the Russia were excited by the wave source over the mid-latitude Atlantic. For example, the wave activity flux is predominantly northeastward from the mid-latitude Atlantic to eastern Russia. This shows that the TAtlSST-related mid-latitude wave source over the Atlantic could have excited a Rossby wave train over Europe and Russia during P3. However, the positive geopotential height anomalies over the Korean

peninsula are not likely to be related to the Rossby wave train from the Atlantic to Russia. For example, the wave activity flux over Korea is mostly eastward, while the Rossby wave train originating from the wave source over the mid-latitude Atlantic is located north of Korea.

The Rossby wave train excited by conditions in the mid-latitude Atlantic, is also clear during P4. The wave activity flux is northeastward from the mid-latitude Atlantic to Scandinavia, and it flows to eastern Russia and northeast Asia. The geopotential height anomalies exhibit negative values over Scandinavia and northwest Asia, and positive values over the eastern Atlantic and western Russia. The Korean peninsula is affected by the negative geopotential height anomaly over northeast Asia; therefore, the geopotential anomaly induces the increased precipitation anomalies. In addition, the negative geopotential height anomaly north of the Korean peninsula leads increased precipitation by inducing a southwesterly wind over Korea. This implies that the Rossby wave train from the mid-latitude Atlantic to the Korean peninsula becomes apparent during P4, which helps to enhance the positive relationship between the TAtlSST and Korean precipitation during boreal summer.

To clearly show that the wave source over the mid-latitude Atlantic is critical to the Rossby wave train from the Atlantic to the Korean peninsula during P4, we performed model experiments using SWM by prescribing the Rossby wave source during P3 and P4 (Schubert et al., 2011). The linearized form of the Rossby wave source (RWS) was calculated as follows (Lim, 2015).

$$RWS_L = -V_\chi' \cdot \nabla(\overline{\zeta} + f) - (\overline{\zeta} + f)\nabla \cdot V_\chi' - \zeta' \nabla \cdot \overline{V}_\chi - \overline{V}_\chi \cdot \nabla \zeta' \qquad (2)$$

where the overbar denotes the 15-yr averaged value and the prime denotes the anomaly associated with the TAtlSST index. The first and fourth term on the right hand of the equation are associated with vorticity advection, while the second and third terms involve the generation of

371 waves by wind convergence/divergence, and the vorticity stretching induced by baroclinic wind
372 anomalies, respectively. In this study, the linearized RWS associated with the
373 convergence/divergence forcing (i.e., second and third terms) is prescribed in the SWM model to
374 focus on the generation of the Rossby wave related to the TAtlSST-related precipitation
375 anomalies (Lim, 2015). In addition, to emphasize the role of the mid-latitude precipitation
376 anomalies, the TAtlSST-related convergence/divergence is prescribed only for 30-40°N and 45-
377 25°W.

378 Figure 8 shows the stream-function anomalies at 500 hPa simulated in SWM with the
379 prescribed mid-latitude RWS related to the TAtlSST index during P3 and P4. Note that only a
380 rotational component of the wind is provided as a result of the SWM, and a positive stream-
381 function (i.e., anti-cyclonic flow) is matched to the positive geopotential height due to the
382 geostrophic balance. With the prescribed forcing during P3, a stationary wave response only
383 shows over the North Atlantic and Western Europe, and the anti-cyclonic flow is weakly
384 simulated north of the Korean peninsula. The overall stream-function response during P3 is
385 much weaker than that during P4, which might be due to the fact that the RWS during P3
386 exhibits much localized pattern than that during P4, which eventually weakens the area-averaged
387 RWS amplitude within the forcing area (i.e. 30-40°N and 45-25°W) (not shown).

388 During P4, stationary wave responses are systematically stronger than during P3. The
389 propagation of the stationary waves from the mid-latitude Atlantic to the Korean peninsula is
390 clearly shown, along with the negative stream-function anomaly over Europe and positive
391 stream-function anomaly over western Russia. In addition, the negative stream-function anomaly
392 centered north of the Korean peninsula is also well-simulated, even though it is shifted slightly
393 north from the observed location. This means that the TAtlSST-related convergence/divergence

anomalies induced by the precipitation anomalies over the mid-latitude Atlantic during P4, can act as a RWS to excite the stationary waves propagated from the mid-latitude Atlantic to the Korean peninsula, which enhances the Tropical Atlantic - Korea (TA-K) teleconnection. The additional SWM experiment by prescribing basic sate during P3 and the RWS during P4 confirms this point that the difference in the RWS, rather than the difference in the basic state, plays a critical role on enhancement of the stream-function response during P4.

Figure 9 shows a schematic diagram of the connection between the tropical Atlantic and Korean precipitation during P3 and P4. There are two pathways (bridges) by which the tropical Atlantic SST could affect Korean precipitation: tropical and extra-tropical. The tropical bridge indicates that the tropical Atlantic warming affects Korean precipitation by inducing variability over the tropical western Pacific. That is, tropical Atlantic warming leads the easterly over the western Pacific by modulating zonal Walker circulation. East of the easterly center, a low-level divergence is induced, which decreases the precipitation over the tropical western Pacific. This excites the anti-cyclonic Rossby waves over the Philippine Sea as a Gill-type response, which leads the southerly over Korea to increase precipitation. Between P3 and P4, the strength of this tropical bridge is enhanced more during P4.

Second, the co-variability between the tropical and mid-latitude SST anomalies over the Atlantic can cause the extra-tropical bridge between the TAtlSST and the Korean peninsula. The TAtlSST-related SST anomalies over the Atlantic exhibit the tripolar SST pattern (Lau and Nath, 2001; Czaja and Marshall, 2001; Czaja and Frankignoul, 2002; Huang and Shukla, 2005; Li et al., 2007), which indicate positive SST anomalies over the tropical, mid-latitude eastern, and northern Atlantic. This co-variability between the tropical and mid-latitude, or north Atlantic warming becomes stronger during P4 than during P3, which enhances positive precipitation

anomalies over the mid-latitude Atlantic during tropical Atlantic warming. The enhanced precipitation anomalies acts as a Rossby wave source, which excites a stationary Rossby wave train propagated from the Atlantic to the Korean peninsula. This extra-tropical wave train generates cyclonic flow over the area north of Korea, which leads a southerly over Korea to increase the precipitation.

4. Summary and Discussion

It was shown that the correlation between the TAtlSST index and Korean precipitation exhibits strong inter-decadal variation, and becomes positive at > 95% confidence level after the 1980s. The intensification of the linkage between the TAtlSST index and Korean precipitation after 1980s is attributed to global warming via the increased background SST. The linear trend of the background SST exhibits stronger SST increase over the Atlantic, eastern Pacific, and the warm-pool region, and it is found that the spatial distribution of SST increases can play a role in enhancing the TA-K teleconnection. The increase in the background SST over the Atlantic provides background conditions that enhance anomalous convective activity due to anomalous SST warming (Choi et al., 2011; Ham and Kug, 2012, 2015, 2016). Therefore, the overall atmospheric responses associated with tropical Atlantic warming are enhanced. In addition, the background SST increases over the warm-pool region also can boost the TA-K teleconnection by leading stronger, low-level convergence feedback (Wang et al., 2000; Hong et al., 2013), which amplifies the TAtlSST-related atmospheric responses over the warm-pool regions.

The correlation between the TAtlSST index and Korean precipitation also exhibits strong inter-decadal variation in 1980–2010, which reaches > 0.8 in 1994–2008, while it is relatively low (i.e., about 0.6) during 1979–1993. It is found that the mid-latitude teleconnection pattern

between the tropical Atlantic and the Korean peninsula becomes robust during 1994–2008 and enhances the TA-K teleconnection. While the mid-latitude SST and precipitation anomalies related to the TAtlSST index are relatively weak for 1979–1993, the co-variability between the tropical and the mid-latitude SST is enhanced systematically in 1994–2008. This generates mid-latitude Rossby wave sources that excite a propagation of stationary waves from the Atlantic to the Korean peninsula through northern Europe and northeast Asia. Due to the stationary waves from the high-latitude route, there is cyclonic flow at the northern edge of the Korean peninsula, which induces an additional southwesterly that increases Korean precipitation. This is supported by a stationary wave model (SWM) experiment prescribing a TAtlSST-related Rossby wave source over the mid-latitude Atlantic during P3 and P4. The results imply that the mid-latitude Rossby wave source is responsible for the observed decadal difference in the TAtlSST-related teleconnection between P3 and P4.

The one of main findings in this study, that the role of inter-annual Atlantic SST variability can be intensified due to global warming, is worth investigating in more detail in future work. While the strength of Atlantic-induced climate variability over other ocean basins could be enhanced due to the global warming through the mechanism proposed in this study; it is also possible that the warming over the Atlantic in the future could be weakened because the strength of Atlantic Meridional Overturning Circulation (AMOC) is expected to weaken in the future (Mikolajewicz et al., 2007; Srokosz et al., 2012; Cheng et al., 2013; Deplazes et al., 2013). Therefore, it is worthwhile to examine whether the active role of the Atlantic climate variability is enhanced as a result of a direct global warming signal, or weakened due to the reduced AMOC strength in the climate model simulations prescribing future emission scenarios.

References

Adler RF, Huffman GF, Chang A, Ferraro R, Xie P, Janowiak J, Rudolf B, Schneider U, Curtis S, Bolvin D, Gruber A, Susskind J, Arkin P, Nelkin E (2003) The version 2 global precipitation climatology project (GPCP) monthly precipitation analysis (1979-present). J Hydrometeorol 4:1147–1167

Annamalai H, Liu P, Xie S-P (2005) Southwest Indian Ocean SST variability: its local effect and remote influence on Asian monsoons. J Clim 18:4150–4167

Chen, X., and T. Zhou, 2014: Relative role of tropical SST forcing in the 1990s periodicity change of the Pacific-Japan pattern interannual variability, *J. Geophys. Res. Atmos*., **119,** 13,043–13,066

Cheng W, Chiang JCH, Zhang D (2013) Atlantic meridional overturning circulation (AMOC) in CMIP5 models: RCP and historical simulations. J Clim 26:7187–7197

Chikamoto Y, Timmermann A, Luo J-J, Mochizuki T, Kimoto M, Watanabe M, Ishii M, Xie S-P, Jin F-F (2015) Skilful multi-year predictions of tropical trans-basin climate variability. Nat Commun 6:6869. doi:10.1038/ncomms7869

Choi J, An S-I, Kug J-S, Yeh S-W (2011) The role of mean state on changes in El Niño's flavor. Clim Dyn 37:1205–1215

Chung P-H, Li T (2013) Interdecadal relationship between the mean state and El Niño types. J Clim 26:361–379. doi:10.1175/JCLID-12-00106.1

Czaja A, Frankignoul C (2002) Observed impact of Atlantic SST anomalies on the North Atlantic Oscillation. J Clim 15:606–623

Czaja A, Marshall J (2001) Observations of atmosphere-ocean coupling in the North Atlantic. Q J R Meteorol Soc 127:1893–1916

Deplazes G, Lückge A, Peterson LC, Timmermann A, Hamann Y, Ka Hughen, Röhl U, Laj C, Ma Cane, Sigman DM, Haug GH (2013) Links between tropical rainfall and North Atlantic climate during the last glacial period. Nat Geosci 6(3):213–217. doi:10.1038/ngeo1712

Ding QH, Wang B, Wallace M, Branstator G (2011) Tropical-extratropical teleconnections in boreal summer: observed interannual variability. J Clim 24:1878–1896

Ding R, Ha K-J, Li J (2010) Interdecadal shifts in the relationship between the East Asian summer monsoon and the tropical Indian Ocean. Clim Dyn 34:1059–1071

Gill AE (1980) Some simple solutions for heat induced tropical circulations. Q J R Meteorol Soc

106:447–462

Ham Y-G, Chikamoto Y, Kug J-S, Kimoto M, Mochizuki T (2017) Tropical Atlantic-Korea teleconnection pattern during boreal summer season. Clim Dyn. doi:10.1007/s00382-016-3474-z

Ham Y-G, Kug J-S (2012) How well do current climate models simulate two types of El Niño? Clim Dyn. doi:10.1007/s00382-011-1157-3

Ham Y-G, Kug J-S (2015) Role of north tropical Atlantic SST on the ENSO simulated using CMIP3 and CMIP5 models. Clim Dyn. doi:10.1007/s00382-015-2527-z

Ham Y-G, Kug J-S (2016) ENSO amplitude changes due to greenhouse warming in CMIP5: Role of mean tropical precipitation in the twentieth century. Geophys Res Lett 43. doi:10.1002/2015gl066864

Ham Y-G, Kug J-S, Kim D, Kim Y-H, Kim D-H (2012) What controls phase locking of ENSO to boreal winter in coupled GCMs? Clim Dyn. doi:10.1007/s00382-012-1420-2

Ham Y-G, Kug J-S, Park J-Y (2013) Two distinct roles of Atlantic SSTs in ENSO variability: north Tropical Atlantic SST and Atlantic Niño. Geophys Res Lett 40:4012–4017. doi:10.1002/grl.50729

Ham Y-G, Kug J-S, Park J-Y, Jin F–F (2013) Sea surface temperature in the north tropical Atlantic as a trigger for El Niño/Southern oscillation events. Nat Geosci 6:112–116. doi:10.1038/ngeo1686

Harris I, Jones PD, Osborn TJ, Lister DH (2013) Updated highresolution grids of monthly climatic observations—the CRU TS3. 10 Dataset. Int J Climatol. doi:10.1002/joc.3711

He C, Zhou T (2014) The two interannual variability modes of the Western North Pacific Subtropical High simulated by 28 CMIP5-AMIP models. Clim Dyn 43:2455–2469. doi:10.1007/s00382-014-2068-x

Ho CH, Kang IS (1988) The variability of precipitation in Korea. J Korean Meteorol Soc 24: 38–48

Hong CC, Chang TC, Hsu HH (2014) Enhanced relationship between the tropical Atlantic SST and the summertime western North Pacific subtropical high after the early 1980s. J Geophys Res. doi:10.1002/2013JD021394

Hong S, Kang I-S, Choi I, Ham Y-G (2013) Climate responses in the tropical Pacific associated with Atlantic warming in recent decades. Asia Pac J Atmos Sci 49:209–217

525 Huang BH, Shukla J (2005) Ocean-atmosphere interactions in the tropical and subtropical
526 Atlantic Ocean. J Clim 18:1652–1672
527 Huang R, Wu Y (1989) The influence of ENSO on the summer climate change in China and its
528 mechanisms. Adv Atmos Sci 6:21–32
529 Jeong J-H, Lee H, Yoo JH, Kwon M, Yeh S-W, Kug J-S, Lee J-Y, Kim B-M, Son S-W, Min S-K,
530 Lee H, Lee W-S, Yoon J-H, Kim H-K (2017) The status and prospect of seasonal climate
531 prediction of climate over Korea and East Asia: A review. Asia Pac J Atmos Sci 53:149-173
532 Kalnay E, Kanamitsu M, Kistler R, Collins W, Deaven D, Gandin L, Iredell M, Saha S,
533 Woollen J, Zhu Y, Chelliah M, Ebisuzaki W, Higgins W, Janowiak J, Mo KC, Ropelewski
534 C, Wang J, Leetma A, Reynolds R, Jenne R, Joseph D (1996) The NCEP/NCAR 40 year
535 reanalysis project. Bull Am Meteorol Soc 77:437–471
536 Kosaka Y, Nakamura H (2006) Structure and dynamics of the summertime Pacific-Japan
537 teleconnection pattern. Q J R Meteorol Soc 132(619):2009–2030. doi:10.1256/qj.05.204
538 Kosaka Y, Xie S-P, Lau N-C, Vecchi GA (2013) Origin of seasonal predictability for summer
539 climate over the Northwestern Pacific. Proc Natl Acad Sci. doi:10.1073/pnas.1215582110
540 Kucharski F et al (2016) Atlantic forcing of Pacific decadal variability. Clim Dyn.
541 doi:10.1007/s00382-015-2705-z
542 Lau N-C, Nath MJ (2001) Impact of ENSO on SST variability in the North Pacific and North
543 Atlantic: seasonal dependence and the role of extratropical sea-air coupling. J Clim 14:
544 2846–2866
545 Lee J-Y, Ha K-J (2015) Understanding of Interdecadal Changes in Variability and Predictability
546 of the Northern Hemisphere Summer Tropical-Extratropical Teleconnection. J Clim
547 28:8634–8647. doi:10.1175/JCLI-D-15-0154.1
548 Lee J-Y, et al., (2017) The long-term variability of Changma in the East Asian summer monsoon
549 system: A review and revisit, Submitted to Asia. Pac. J. Atmos.
550 Li S, Robinson WA, Hoerling MP, Weickmann KM (2007) Dynamics of the extratropical
551 response to a tropical Atlantic SST anomaly. J Clim 20(3):560–574
552 Li X, Xie S-P, Gille ST, Yoo C (2016) Atlantic-induced pan-tropical climate change over the
553 past three decades. Nat Clim Change 6:275–279
554 Lim, Y.-K., K.-Y. Kim, and H.-S. Lee (2002) Temporal and spatial evolution of the Asian
555 summer monsoon in the seasonal cycle of synoptic fields. *J. Climate*, **15**, 3630-3644.

556 Lim Y-K (2015) The East Atlantic/West Russia (EA/WR) teleconnection in the North Atlantic:
557 climate impact and relation to Rossby wave propagation. Clim Dyn 44:3211–3222.
558 doi:10.1007/s00382-014-2381-4
559 Liu AZ, Ting M, Wang H (1998) Maintenance of circulation anomalies during the 1988 drought
560 and 1993 floods over the United States. J Atmos Sci 55:2810–2832
561 McGregor S et al (2014) Recent Walker circulation strengthening and Pacific cooling amplified
562 by Atlantic warming. Nat Clim Change 4(10):888–892
563 Mikolajewicz U, Vizcaino M, Jungclaus J, Schurgers G (2007) Effect of ice sheet interactions in
564 anthropogenic climate change simulations. Geophys Res Lett 34:L18706.
565 doi:10.1029/2007GL031173
566 Rodionov SN (2004) A sequential algorithm for testing climate regime shifts. Geophys Res Lett
567 31. doi:10.1029/2004GL019448
568 Rong X, Zhang R, Li T (2010) Impacts of Atlantic sea surface temperature anomalies on Indo-
569 East Asian summer monsoon-ENSO relationship. Chin Sci Bull 55:2458–2468
570 Schubert S, Wang H, Suarez M (2011) Warm season subseasonal variability and climate
571 extremes in the Northern Hemisphere: the role of stationary Rossby waves. J Clim 24:4773–
572 4792
573 Seo K-H, Son J-H, Lee J-Y (2011) A new look at changma: atmosphere. Korean Meteor Soc
574 21:109–121
575 Smith T, Reynolds R, Peterson T, Lawrimore J (2008) Improvements to NOAA's historical
576 merged land–ocean surface temperature analysis (1880–2006). J Clim 21:2283–2296.
577 doi:10.1175/2007JCLI2100.1
578 Son H-Y, Park J-Y, Kug J-S, Yoo J, Kim C-H (2014) Winter precipitation variability over
579 Korean Peninsula associated with ENSO. Clim Dyn 42:3171–3186
580 Son HY, Park JY, Kug JS (2015) Precipitation variability in September over the Korean
581 Peninsula during ENSO developing phase. Clim Dyn. doi:10.1007/s00382-015-2776-x
582 Srokosz M, Baringer M, Bryden H, Cunningham S, Delworth T, Lozier S, Marotzke J, Sutton R
583 (2012) Past, present and future change in the Atlantic meridional overturning circulation.
584 Bull Amer Meteorol Soc. doi:10.1175/BAMS-D-11-00151.1
585 Steinman BA, Mann ME, Miller SK (2015) Atlantic and Pacific multidecadal oscillations and
586 Northern Hemisphere temperatures. Science 347(6225):988–991.

587 doi:10.1126/science.1257856
588 Takaya K, Nakamura H (2001) A formulation of a phase-independent wave-activity flux for
589 stationary and migratory quasigeostrophic eddies on a zonally varying basic flow. J Atmos
590 Sci 58:608–627
591 Wang B, Jhun J-G, Moon B-K (2007) Variability and singularity of Seoul, South Korea, rainy
592 season (1778–2004). J Clim 20:2572-2580
593 Wang B, Wu R-G, Fu X-H (2000) Pacific-east Asian teleconnection: How does ENSO affect
594 Asian climate? J Clim 13:1517–1536
595 Wang C (2000) On the atmospheric responses to tropical Pacific heating during the mature phase
596 of El Nino. J Atmos Sci 57:3767-3781
597 Wang H, Wang B, Huang F, Ding Q, Lee JY (2012) Interdecadal change of the boreal summer
598 circumglobal teleconnection (1958–2010). Geophys Res Lett 39:L12704.
599 Wu R, Yang S, Liu S, Sun L, Lian Y, Gao Z (2011) Northeast China summer temperature and
600 North Atlantic SST. J Geophys Res 116:D16116. doi:10.1029/2011JD015779
601 Wu R, Yang S, Liu S, Sun L, Yi L, Gao Z (2010) Changes in the relationship between Northeast
602 China summer temperature and ENSO. J Geophys Res 115:D21107.
603 doi:10.1029/2010JD014422
604 Yang J, Liu Q, Xie S-P, Liu Z, Wu L (2007) Impact of the Indian Ocean SST basin mode on the
605 Asian summer monsoon. Geophys Res Lett 34:L02708. doi:10.1029/2006GL028571
606 Ye K, Wu R, Liu Y (2015) Interdecadal change of Eurasian snow, surface temperature, and
607 atmospheric circulation in the late 1980s. J Geophys Res 120:2738–2753.
608 doi:10.1002/2015JD023148
609 Yun K-S, Lee J-Y, Ha K-J (2014) Recent intensification of the South and East Asian monsoon
610 contrast associated with an increase in the zonal tropical SST gradient. J Geophys Res
611 Atmos 119:8104–8116
612
613
614

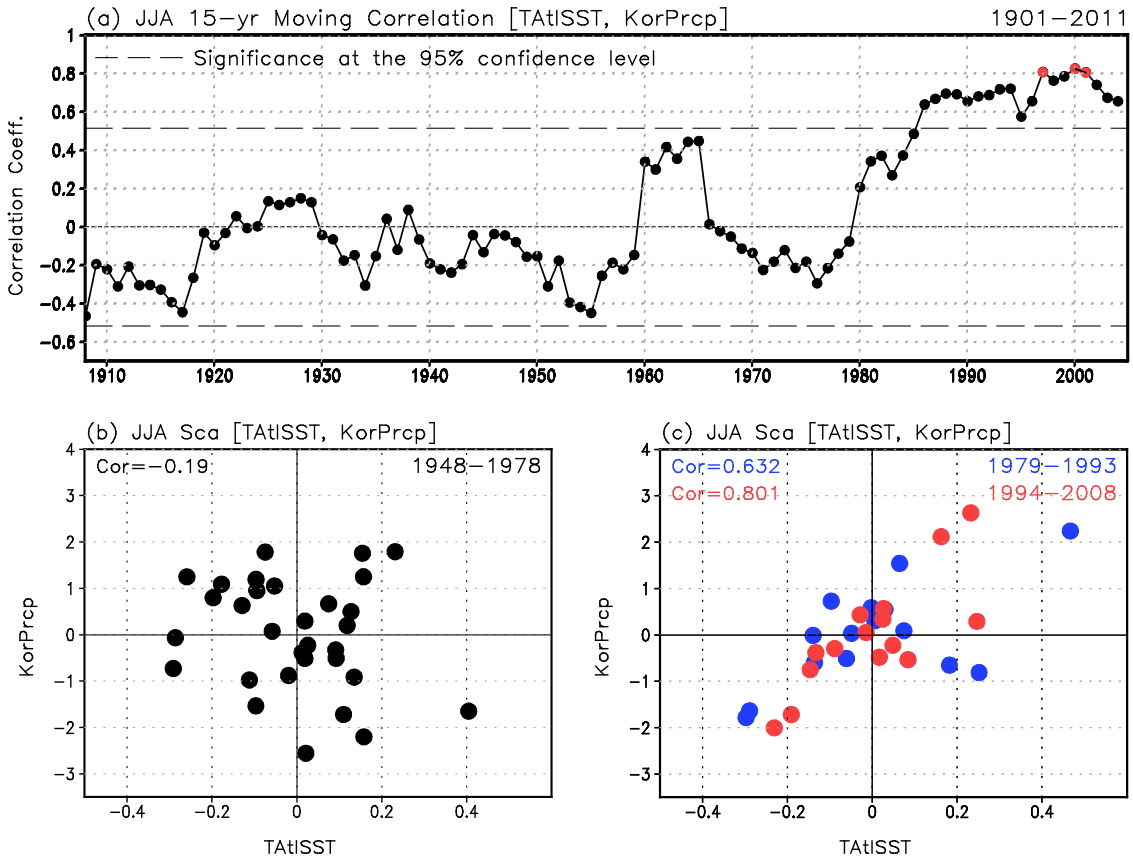

615

616

617 Figure 1. (a) The 15 yr moving correlation between precipitation anomalies over the Korean
618 peninsula (35–40° N, 120–130° E) and Tropical Atlantic SST (60° W to 20° E and 30° S to 30°
619 N; TAtlSST) during Korean summer (June-July-August: JJA) from 1901 to 2011. The dashed
620 line indicates statistical significance at the 95% confidence level by the Students' t-test. (b) A
621 scatter diagram of the precipitation anomalies over the Korean peninsula and TAtlSST anomalies
622 during JJA, from 1948 to 1978. (c) As in (b), but the black dots indicate 1979–2010, the blue
623 dots 1979–1993, and the red dots 1994–2008.

624

625

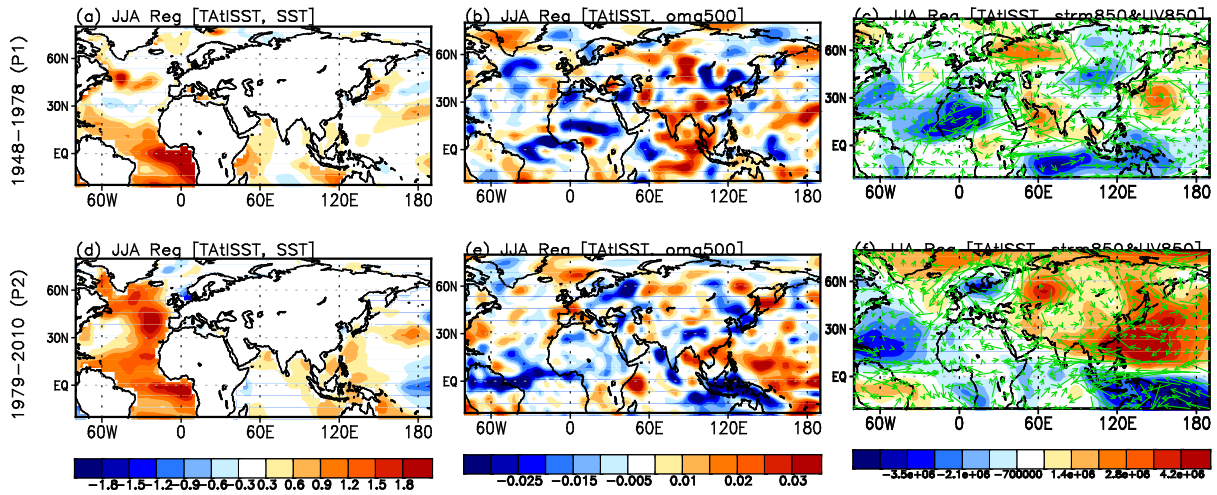

Figure 2. Regression maps of (a, d) SST (K/K), (b, e) Vertical pressure velocity at 500 hPa (hPa/K), (c, f) Stream function (shaded, $m^2/s/K$) and horizontal wind anomalies at 850 hPa (vector, m/s/K) onto the TAtlSST index during JJA of 1948–1978 (upper, P1) and 1979–2010 (lower, P2).

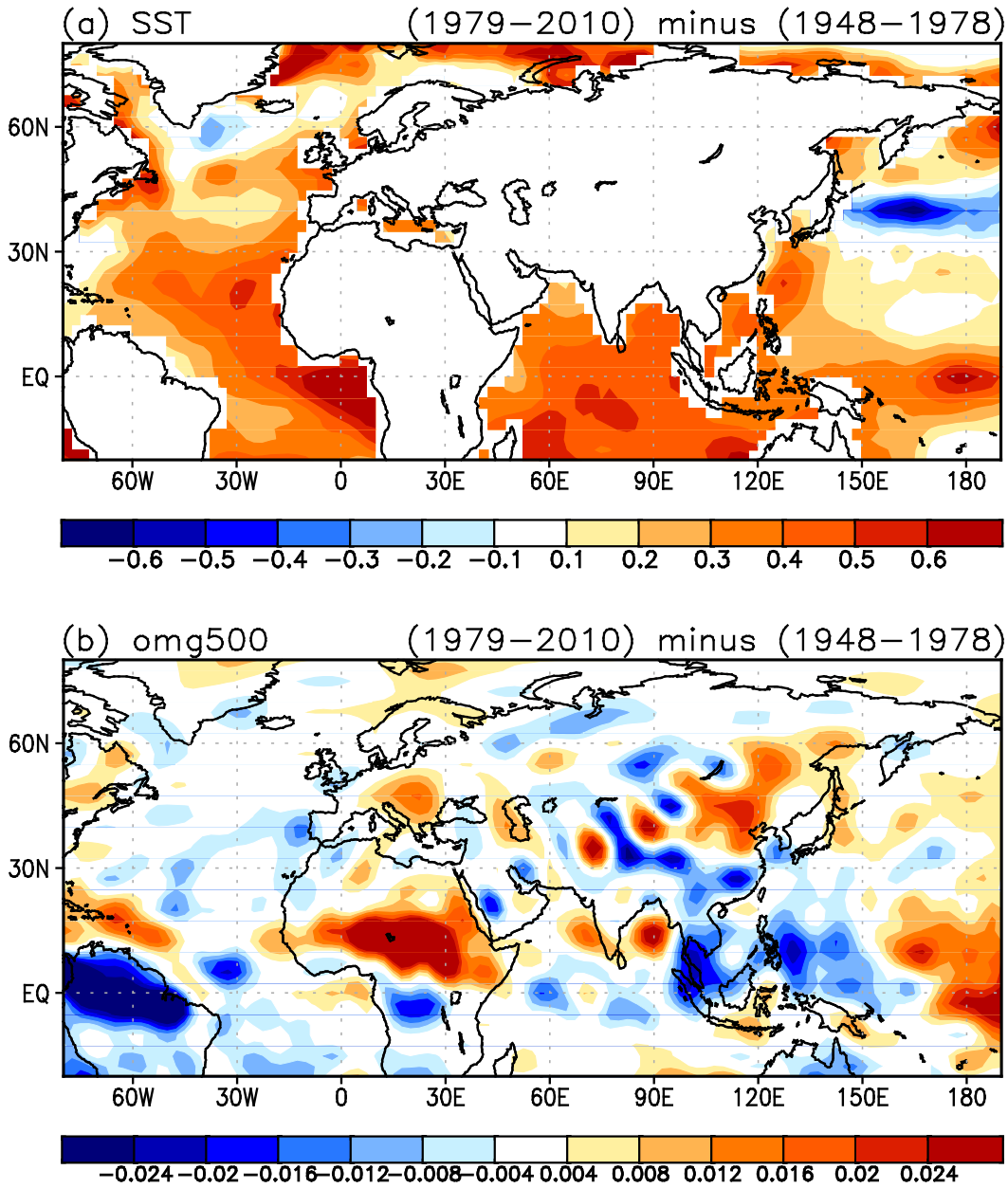

631
632

633 Figure 3. Difference in background (a) SST and (b) Vertical pressure velocity at 500 hPa during
634 1979–2010 (P2) from that during 1948–1978 (P1).

635

636

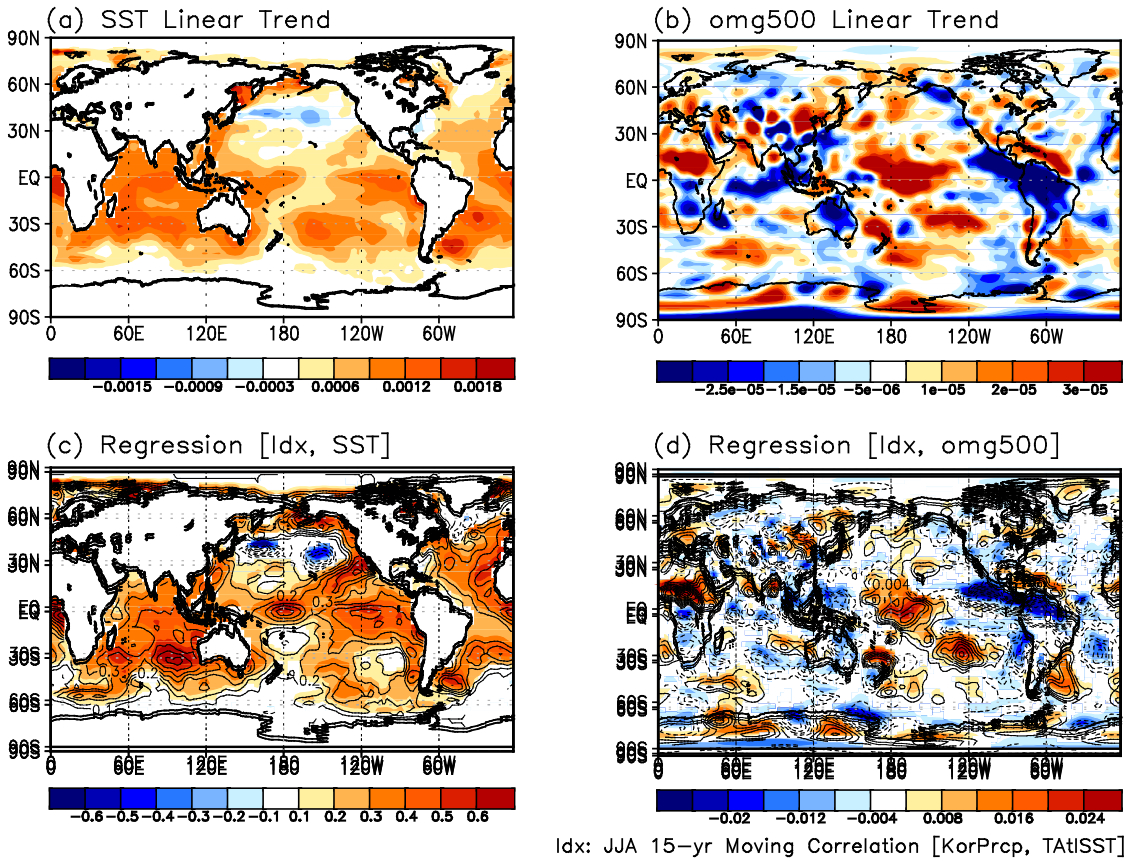

Figure 4. Linear trend of the background (a) SST and (b) Vertical pressure velocity at 500 hPa from 1948 to 2010: Linear regression maps of (c) SST and (c) Vertical pressure velocity at 500 hPa onto the 15-yr moving correlation between the TAtlSST index and Korean precipitation from 1948 to 2010. In panel (c) and (d), the regions over 95% confidence level with student t-test are shaded.

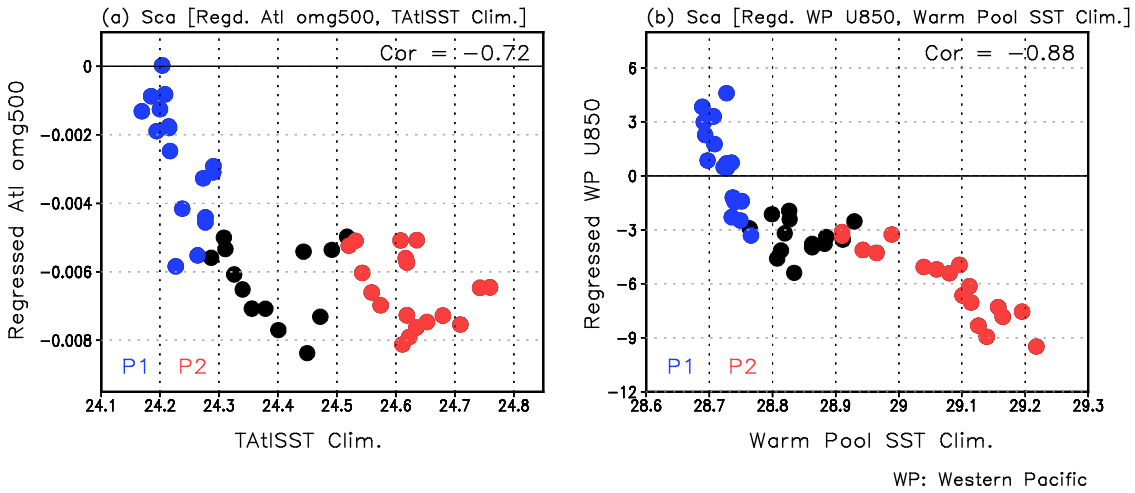

Figure 5. (a) A Scatter diagram between the 15-yr moving SST over the tropical Atlantic region (30° S to 30° N and 60° W to 20° E,) and the regressed vertical pressure velocity over the tropical Atlantic (20° S to 30° N and 60° W to 20° E) onto the TAtlSST index from 1948 to 2010. (b) A scatter diagram between the 15-yr moving SST over the warm pool region (5° S to 10° N and 100–140° E,) and the regressed zonal wind at 850 hPa over the western Pacific (5° S to 10° N and 130–160° E; WP) onto the TAtlSST index from 1948 to 2010.

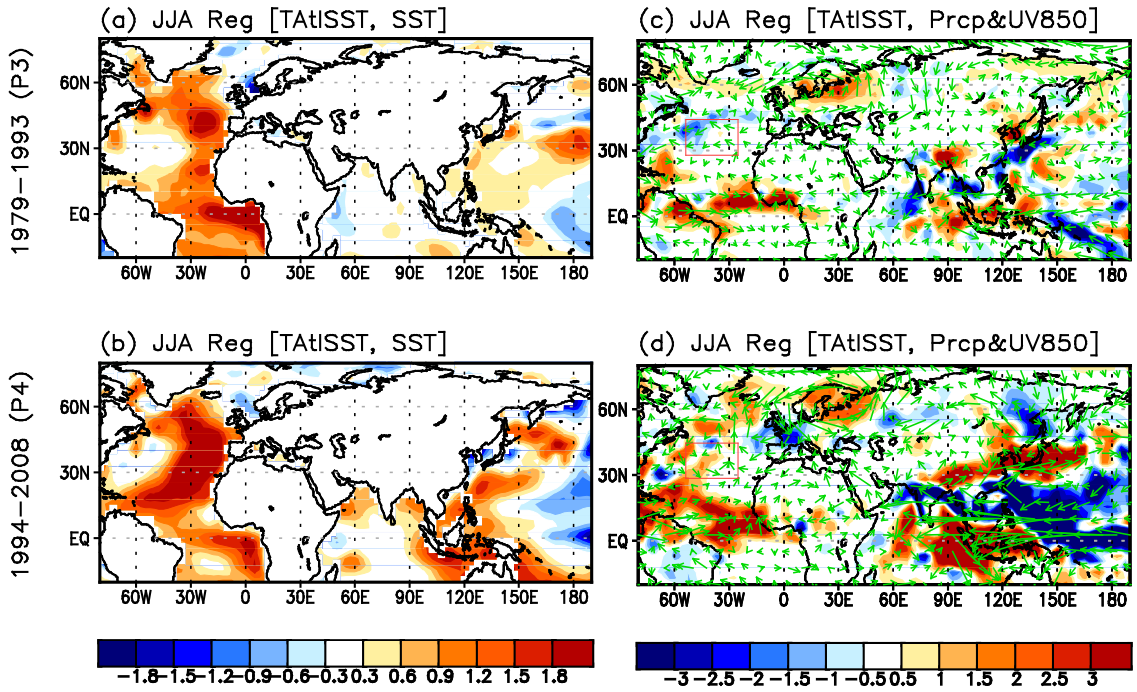

Figure 6. Regression maps of (a, b) SST (K/K); (c, d) Precipitation (shaded, mm/day/K) and horizontal wind anomalies at 850 hPa (vector, m/s/K) onto the TAtlSST index during JJA of 1979–1993 (upper, P3) and 1994–2008 (lower, P4).

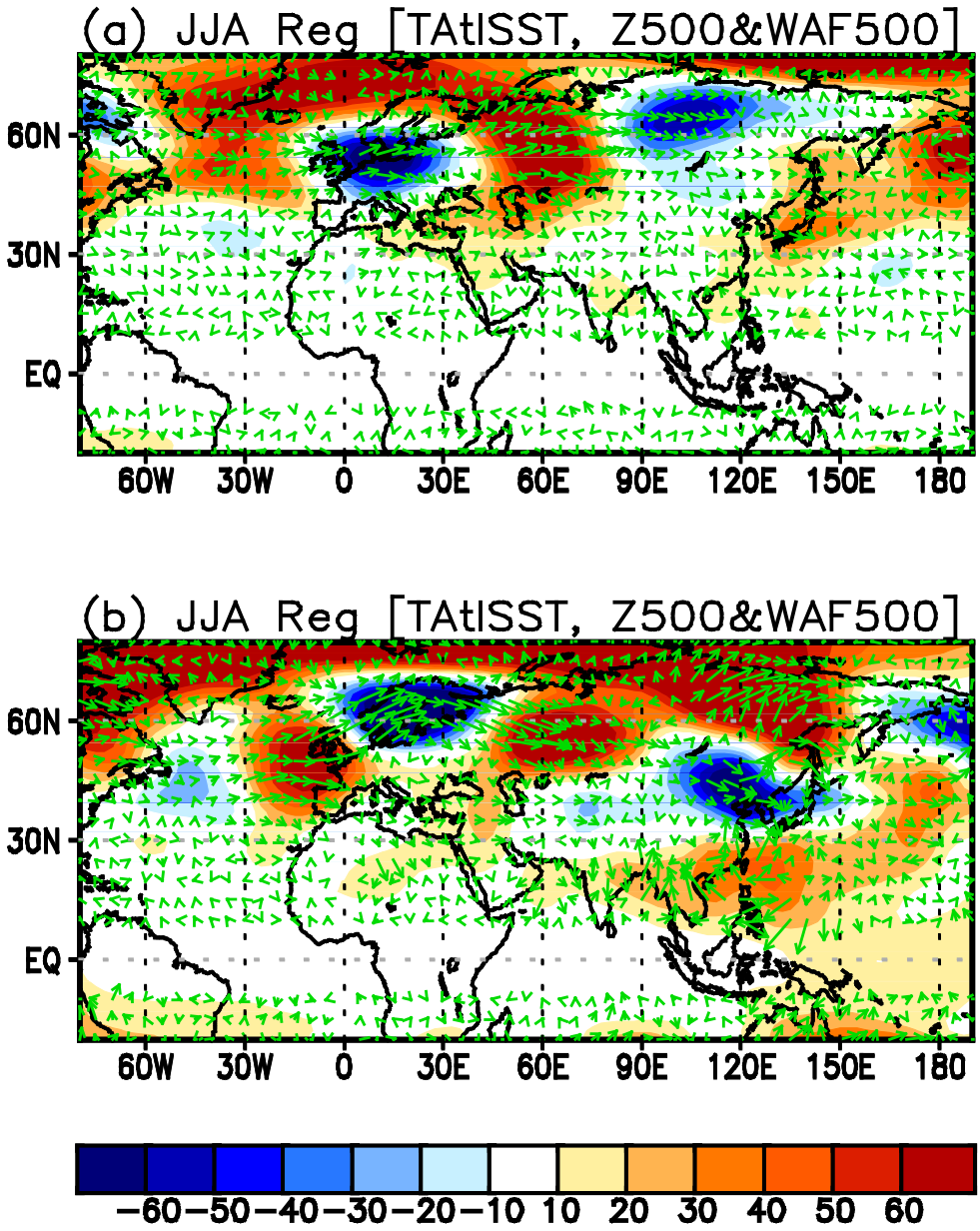

662
663 Figure 7. Regression maps of geopotential height at 500 hPa (shaded) and wave activity flux at
664 500 hPa (vector) onto the TAtlSST index during JJA of (a) 1979–1993 (P3) and (b) 1994–2008
665 (P4).
666

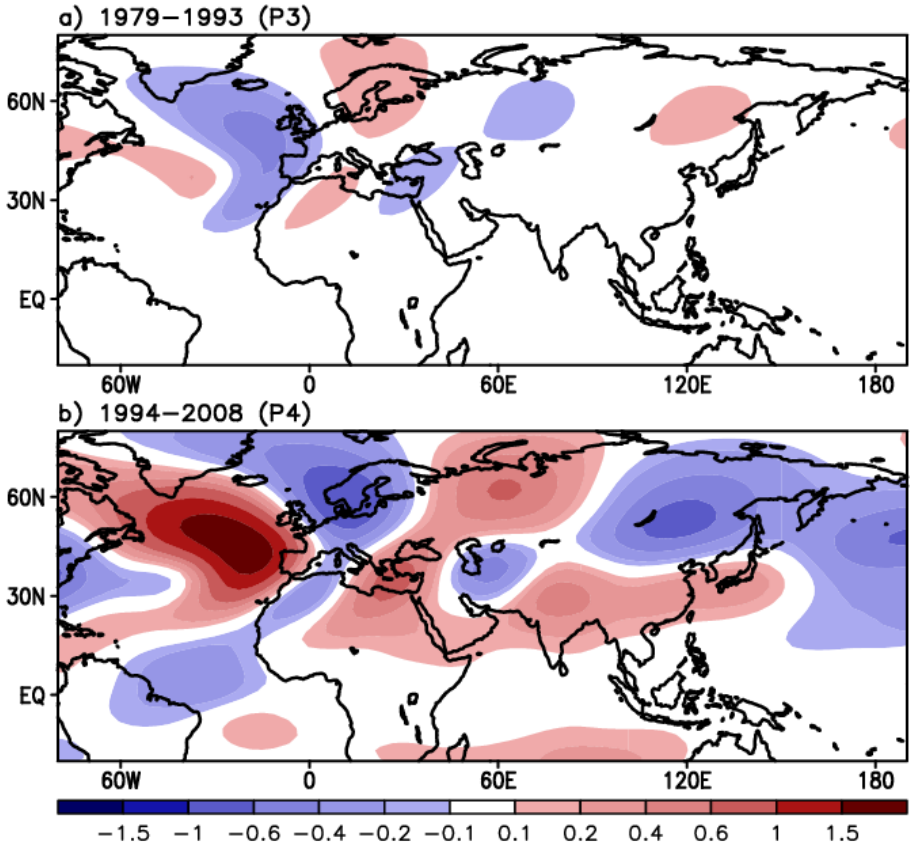

667

668 Figure 8. Stream-function anomalies at 500 hPa simulated in a stationary wave model (SWM)
669 with the prescribed mid-latitude Rossby wave source related to TAtlSST index during (a) 1979–
670 1993 (P3) and (b) 1994–2008 (P4). The linearized RWS is prescribed only over the mid-latitude
671 eastern Atlantic (30–40° N and 45–25° W).

672

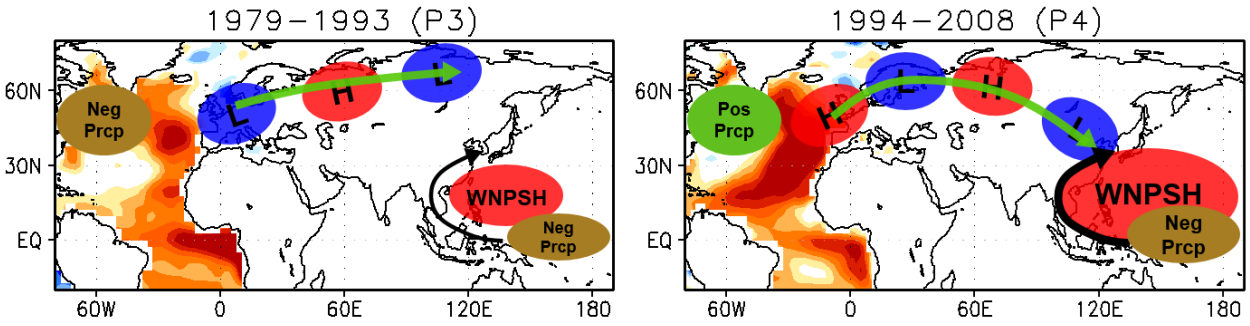

Figure 9. Schematic diagram of the connection between the tropical Atlantic and Korean precipitation for 1979–1993 (P3) and 1994–2008 (P4). Shading over the Atlantic shows anomalous SST warming related to the TAtlSST index. The small red/blue circles show anomalous high/low pressure at 500 hPa, and the large red circle over the western Pacific represents the western-north Pacific subtropical high (i.e., WNPSH). The green/brown circles show anomalous positive/negative precipitation. The green vector represents the wave activity flux and black vector represents the low-level wind. The Rossby wave train from the mid-latitude Atlantic to Korean peninsula (green vector) becomes apparent along with the stronger intensity of the WNPSH during P4. Both lead a stronger southerly over the Korean peninsula (black vector) to enhance the TAtlSST-related precipitation anomalies over Korea during P4.